Composites Part B 162 (2019) 425–432

Contents lists available at ScienceDirect

Composites Part B

journal homepage: www.elsevier.com/locate/compositesb

Effect of APTMS modification on multiwall carbon nanotube reinforced epoxy nanocomposites

Kunal Mishra[a,*], Raman P. Singh[a,b]

[a] School of Mechanical and Aerospace Engineering, USA
[b] School of Material Science and Engineering, 526 N. Elgin Av., Oklahoma State University, Tulsa, OK, 74106, USA

ARTICLE INFO

Keywords:
CNT
Silane modification
Fracture toughness
AFM
SEM
Elastic modulus

ABSTRACT

In this present investigation, we have studied the effect of chemical functionalization, and mechanical dispersion of carbon nanotube (CNT) reinforced epoxy resin. The chemical function of the CNT has been done by silane treatment. Silane modification has been done first by acid treatment on ball-milled CNT followed by chemical treatment of amine-based silane. FTIR spectra exhibit that silane chemically interacts with the CNT and epoxy resin. Mechanical dispersion of CNT in the epoxy was performed in the planetary ball mill. Ball milled CNT shows some degree of exfoliation. Mechanical properties of ball-milled and silane modified CNT reinforced epoxy is characterized in terms of fracture toughness and tensile modulus. Silane-modified CNT/epoxy shows an increase of 38% and 42% compared to the neat resin for fracture toughness and tensile modulus values respectively. Increase in the mechanical properties for silane modified CNT/epoxy is due to the excellent adhesion between CNT-matrix as well as significant dispersion of CNT in the epoxy resin provided by silane molecule as observed from TEM images. AFM indentation on the nanocomposites exhibits the presence of CNT agglomerates through adhesion and corresponding modulus map at the nanoscale level. SEM images indicate an increase in surface roughness with CNT inclusion which relates to the existence of an extrinsic mechanism. Additionally, better adhesion between CNT and matrix due to silane modification indicate a higher T_g value of silane modified CNT/epoxy than ball milled CNT/epoxy.

1. Introduction

Carbon nanotube (CNT) due to their novel carbon–carbon architecture with their notably high aspect ratio leads to the exceptional mechanical, electrical and thermal properties that make them the ideal candidate for strengthening the material. From past some decades, an extensive amount of the research has been done on the CNT reinforced epoxy nanocomposites. Increase in the thermal, mechanical and electrical properties have been reported on these nanocomposites with the inclusion of CNT [1–3]. However, CNTs tend to bundle up even at lower weight reinforcement and form agglomerates that eventually lead to the deleterious consequences on the nanocomposites [4,5]. The comprehensive study has been done to improve the dispersion of the CNT in the polymer matrix. Better dispersion has been achieved by two methods, namely the mechanical dispersion of CNT and functionalization of the surface of the CNT. The high energy provided during mechanical dispersion, such as ultrasonication, ball milling, and high shear mixing, is used to break the agglomerates. Functionalization of the surface of CNT has been done to achieve the proper dispersion as well as providing the better interface between CNT and polymer matrix [6–9]. However, using highly acidic or basic chemicals to functionalize the surface of CNT cause damage to the CNT surface. Functionalization with the organosilanes is one of the newer functionalization techniques that researchers have worked on because of moderate chemical interaction of silanes with the CNT. Silanes due to their unique two-reactive-side serves as an adhesion promoter between CNT and the polymer matrix [10–14]. One molecule of the organosilane contains two reactive group; one is the functional part that can react with the polymer chain while hydrolyzable group can condense with hydroxyl group of the CNT. This condensation of hydroxyl group on the surface of CNT prevents the van der Waal attractions between the CNT [15]. In the recent past, researchers have investigated the various silanization technique on the CNTs with great results. Modification of CNT with amine and epoxide based silanes have shown exceptional improvement in thermomechanical properties [16,17]. Even though most of the studies have demonstrated the effect of chemical functionalization of CNT on the *bulk properties* of the nanocomposites. However, the investigation of the influence of chemical functionalization on the mechanical

* Corresponding author.
E-mail address: kunalm@okstate.edu (K. Mishra).

https://doi.org/10.1016/j.compositesb.2018.12.134
Received 20 June 2018; Received in revised form 27 December 2018; Accepted 30 December 2018
Available online 03 January 2019
1359-8368/

properties of CNT reinforced nanocomposites at *micro* or *nano scale* is critical. Transmission electron microscopy can be used to determine the properties at nanoscale qualitatively, but the robust method to determine the properties quantitatively is significant. As the properties at micro or nano-level significantly govern the overall bulk properties of these nanocomposites. This study investigates the consolidated effect of mechanical dispersion, and chemical functionalization on mechanical and thermal properties of the CNT reinforce epoxy resin. We have used the unique method of determining the mechanical and adhesion properties of nanocomposite from atomic force microscopy. Force mapping was done to generate "full-field" load-displacement indentation and adhesion curve simultaneously and synergistically.

2. Materials and fabrication

The polymer system adopted in this work consists of diglycidyl ether of bisphenol-F based resin (EPON 862®, Hexion Specialty Chemicals, Columbus, OH), that is cured with a low viscous aliphatic amine (EPIKURE 3274 ® Hexion Specialty Chemicals, Columbus, OH). Both the resin and the curing agent were acquired from Miller-Stephenson Chemical Company, (Danbury, CT). This epoxy resin system is a highly cross-linked network that results in excellent mechanical properties and high chemical resistance. The multiwall carbon nanotubes, of an average diameter of 10 nm were acquired from Sigma Aldrich (St. Louis, MO). (3-Aminopropyl) trimethoxysilane (APTMS) was also obtained from Sigma-Aldrich (St. Louis, MO).

To break the CNT agglomerates and increase the surface area of CNT as shown in Fig. 1 following process has been done: CNT was first placed inside in a Retsch (Dusseldorf, Germany) PM 200 planetary ball mill for 60 min at 200 rpm. The ratio of the weight of balls used in the ball milling machine to the CNT is 10:1. Ball milled CNT was then added to a beaker filled with 100 ml of isopropyl alcohol (IPA) for ultrasonication using the ultrasonic disrupter (TM750, Tekmar-Dhormann, Cincinnati, OH), operating at 20 kHz frequency with 5 s on-off cycle, for 30 min. During the ultrasonication, the mixture was placed in an ice bath to maintain the uniform temperature of approximately 70 °C.

Chemical modification of the CNT, as shown in Fig. 2, was performed by treating ball-milled CNT with APTMS by initially dispersing the 2g of CNT in an acid solution (100 ml of H_2SO_4 and 150 ml of HNO_3) at 50 °C for 5 h, followed by filtering with distilled water and washing with isopropanol so that pH of CNT reached between 6 and 7. The resulting CNTs were then dried at 75 °C. It was dispersed in APTMS-ethanol solution (2:98 v/v), followed by mixing of the solution at 70 °C for 6 h to evaporate the alcohol. Two different set of CNT–epoxy nanocomposites were prepared namely ball milled (B-CNT), and APTMS modified CNT (A-CNT) at loading levels of 0.1%, 0.25%, 0.5%, 1%, and 2%.

To fabricate CNT reinforced epoxy nanocomposites, the CNT was added slowly to epoxy operated at 50 °C, while processing at the magnetic mixer. After 1 h of mechanical mixing, the mixture was placed in an ice bath to maintain the steady temperature around 70 °C, and high energy agitation is provided by an ultrasonic disrupter using a 20 kHz frequency and a 5.0 s on-off cycle for 20 min.

The mixture was then cooled to room temperature, and 40% wt. of the amine-based curing agent (EPIKURE 3274) were added in the stoichiometric quantity to epoxy resin followed by mixing for 10 min. Subsequently, the mixture was placed in a vacuum chamber for 30 min for degassing. The degassed mixture was poured into a pre-prepared mold for casting and cured at room temperature for 24 h. The cast plate was then released from the mold and post cured at 121 °C for 6 h. The same procedure was used for preparing neat resin samples for comparison.

2.1. Characterization

Fracture toughness was determined using single edge notch bend testing as per ASTM D–5045 [18]. Samples were machined from the cast plate with nominal dimensions of 54.0 × 12.7 × 6.3 mm. A 4.5 mm deep notch was cut using a diamond precision saw, and then the tip of the notch was tapped lightly with a razor blade to initiate a natural pre-crack. The nominal crack length was maintained between 5.7 and 6.9 mm to maintain as a/W ratio of 0.45–0.55 as per the ASTM standard. The pre-cracked single edge notch specimens were loaded under three-point bending using a universal testing machine (Instron 5567, Norwood, MA). Tests were conducted in a displacement-controlled mode at a fixed crosshead speed of 0.5 mm/min till the point of specimen failure. Failure was identified by reaching a peak value of the applied load. The fracture toughness of the nanocomposites was then estimated in terms of the critical stress intensity factor (K_{IC}) calculated from the peak load.

The elastic modulus of the CNT/epoxy nanocomposites was determined as per ASTM D–638 [19]. Samples were machined from cast plate with nominal dimension for Type 1 specimen (thickness less than 7 mm) as per ASTM standard. Extensometer was set within the gauge length to register the actual change in distance between two points when the specimen is pulled. Tests were conducted in a displacement-controlled mode at a fixed crosshead speed of 0.1 mm/min till the point of specimen failure. The elastic modulus was determined from the stress-strain curve. Experimental values of the elastic modulus were compared with theoretical values of elastic modulus using Hashin-Shtrikman model (H–S model) [20]. H–S bounds for Young's modulus were calculated for a two-phase material.

$$E_x^* = \frac{9K_x^*G_x^*}{3K_x^* + G_x^*} \tag{1}$$

where K_x^*, represents the bulk modulus and G_x^* represents shear modulus, whereas $x = U$ and $x = L$ represents the upper and lower bound values.

$$K_L^* = K_1 + V_2\left(\frac{1}{K_2 - K_1} + \frac{3V_1}{3K_1 + 4G_1}\right)^{-1}, \tag{2a}$$

$$K_U^* = K_2 + V_1\left(\frac{1}{K_1 - K_2} + \frac{3V_2}{3K_2 + 4G_2}\right)^{-1}, \tag{2b}$$

$$G_L^* = G_1 + V_2\left(\frac{1}{G_2 - G_1} + \frac{6V_1(K_1 + 2G_1)}{5G_1(3K_1 + 4G_1)}\right)^{-1}, \tag{2c}$$

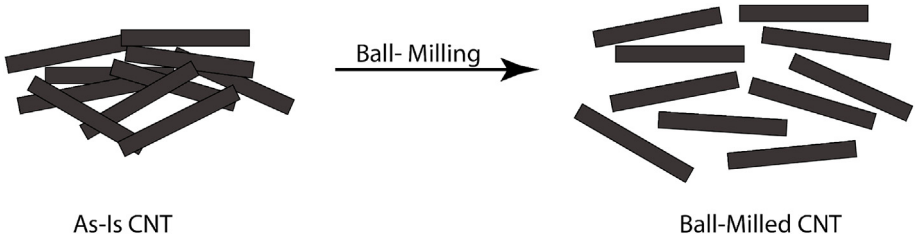

Fig. 1. Ball milling of the CNT will leads to breaking of the agglomerates and increasing the surface area of CNT.

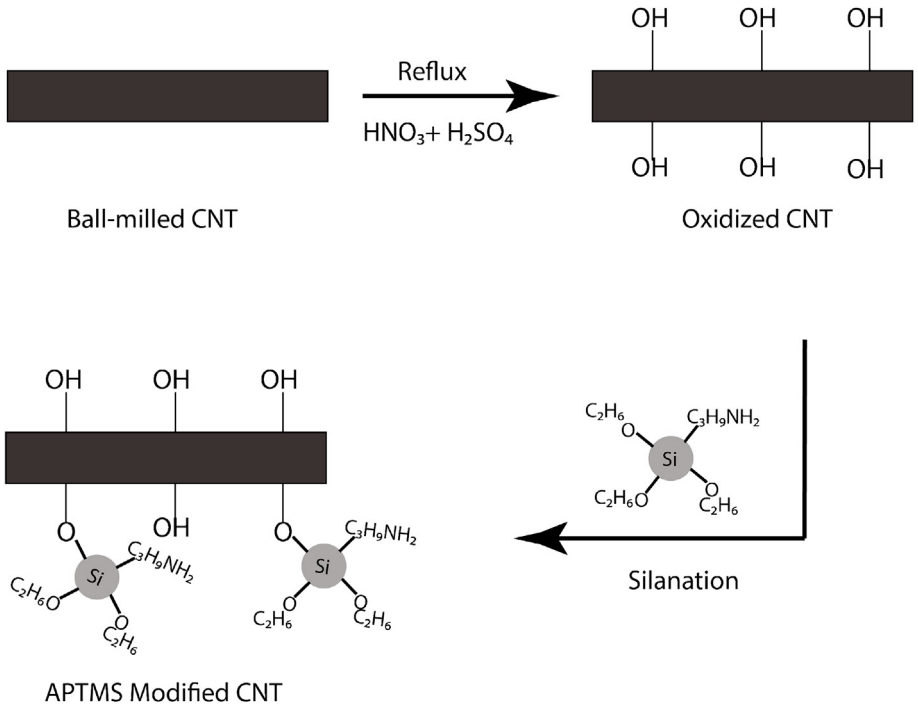

Fig. 2. Process of silane modification of ball-milled CNT.

$$G_U^* = G_2 + V_1\left(\frac{1}{G_1 - G_2} + \frac{6V_2(K_2 + 2G_2)}{5G_2(3K_2 + 4G_2)}\right)^{-1}, \tag{2d}$$

Whereas K, G, and V are the bulk modulus, shear modulus and weight fractions, respectively. It must be noted that subscript 1 and subscript 2 is used for the matrix and fillers respectively. The Young's modulus and Poisson's ratio of the epoxy resin were selected 3 GPa and 0.33 respectively from the literature. The Young's Modulus and Poisson's ratio of the multiwall CNT used in this study were advised by the manufacturer which is around 700 GPa and 0.31 respectively. The bulk modulus and shear modulus of the epoxy resin was determined from the elastic modulus and Poisson's ratio.

$$K = \frac{E}{3(1 - 2\nu)} \tag{3a}$$

$$G = \frac{E}{2(1 + \nu)} \tag{3b}$$

Thermal analysis of samples was carried out using a differential scanning calorimeter (Q 2000 DSC, TA Instruments, Inc., New Castle, DE), to study the glass transition temperature (T_g). The instrument was calibrated by employing the temperature and heat of fusion of high purity Indium standard. The thermal histories of all the nanocomposites were maintained the same before each experiment. Approximately 5–10 mg of sample was loaded in an aluminum pan. The samples were first heated to 210 °C at a scan rate of 10 °C/min, held at that temperature for 2 min. To eliminate any previous thermal history, and then cooled to −25 °C at a cooling rate of 10 °C/min. For the second scan, the samples were heated and cooled under the same conditions. The data was obtained from the second heating cycle. The experiment was carried out in under constant nitrogen flow (flow rate 50 ml min^{-1}).

The fractured surface was studied using field emission scanning electron microscopy (Hitachi S-4800 FESEM, Dallas, TX). Before imaging, the surfaces of the samples were coated with gold-platinum by an electro-deposition method utilizing a sputter coater (Cressington Scientific Instruments Ltd, Redding, CA) to make the sample conductive to prevent the accumulation of static electric charge during scanning electron microscopy.

Fourier transform infrared spectroscopy (FTIR) was performed to investigate the variation in chemical interactions with silane modification. The materials were powdered using an industrial grinder under liquid nitrogen. These powdered samples were loaded in an FTIR spectrometer (Nicolet iS10, Waltham, MA) and subjected to 128 scans at a resolution of 4.0 cm^{-1}. The spectrum of interest was collected at room temperature between 4000 and 500 cm^{-1}.

Transmission electron microscopy (TEM) (EOL JEM-100CX II, Peabody, MA) was used to identify and characterize agglomeration phenomena in CNT/epoxy nanocomposites. All samples were ultramicrotome (Reichert-Jung Ultracut E, Dickinson, TX) to 70 nm thicknesses using a diamond knife. Slices were mounted on amorphous-carbon-coated copper TEM grids.

Atomic force microscopy (AFM) indentation on the CNT reinforced samples were conducted to study the elastic modulus value at the microscale level. For sample preparation of AFM, small circular blocks of samples were cut using precision cutter (ISOMET 1000, Buehler, Lake Bluff, Illinois) and polished using metallographic methods starting from 320 grit grinding paper to 0.05 μm alumina particles using an automated polisher (Labopol 5, Struers, Cleveland, Ohio, USA). The surface roughness of the samples was kept below than 5 nm because the indentation depths need to be higher than the surface roughness to avoid the influence of surface artifacts (such as pile up or sink in). An atomic force microscope (MFP–3D, Asylum Research, Santa Barbara, CA, USA) was used for conducting AFM indentations on the prepared samples. The AC160TS AFM indenter tip, manufactured by Olympus Micro Probes (Center Valley, PA, USA), which is recommended for the study of polymers and filler reinforced composites, was used for indentation. It has a resonant frequency of 300 kHz and spring constant of 42 N/m. The indentation was done on a polymer (Polymethyl methacrylate) of known modulus to calibrate the initial parameters and identify the values used for AFM. Using the contact mode, force maps were generated at each position covered with 48 by 48 grid across a square region of 5μm.

3. Results and discussion

Fig. 3 exhibits the spectra of B-CNT/epoxy and A-CNT/epoxy, the

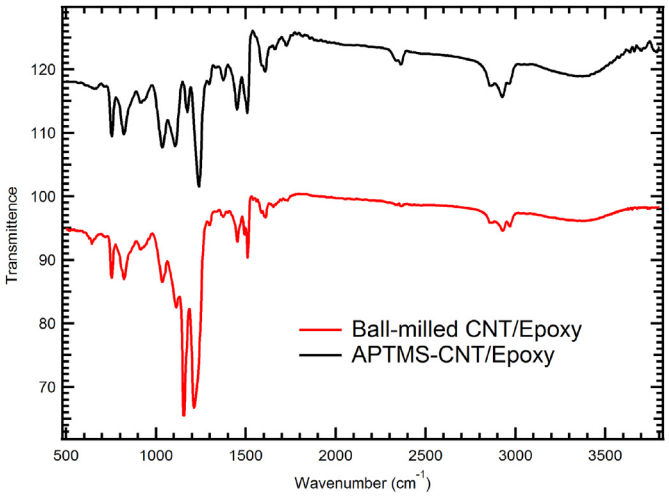

Fig. 3. Spectra of A-CNT/epoxy and B-CNT/epoxy shows change in the peak witl silane modification.

small peaks around 1600 cm^{-1} indicates the presence of -NH group and presence of strong peak around 1160 cm^{-1} suggests the presence of Si-O group imply that the APTMS chemically interact with the epoxy and CNT.

Fig. 4 illustrates the load-displacement graph corresponding to the fracture experiments for neat resin and materials containing 0.5 wt% CNT reinforcement. This load-displacement data was obtained from specimens of similar crack lengths to aid comparison. It must be noted that silane modification of the CNT results in a higher resistance against crack propagation compares to neat resin and B-CNT. This variation in load–displacement graph is further supported by fracture toughness results.

Fig. 5 shows the variations in the value of fracture toughness as a function of CNT loading. As explained earlier, the fracture toughness was estimated in terms of the value of the critical stress intensity factor at the initiation of crack growth. The error bars in the figure signify the statistical spread of experimental data in terms of the standard

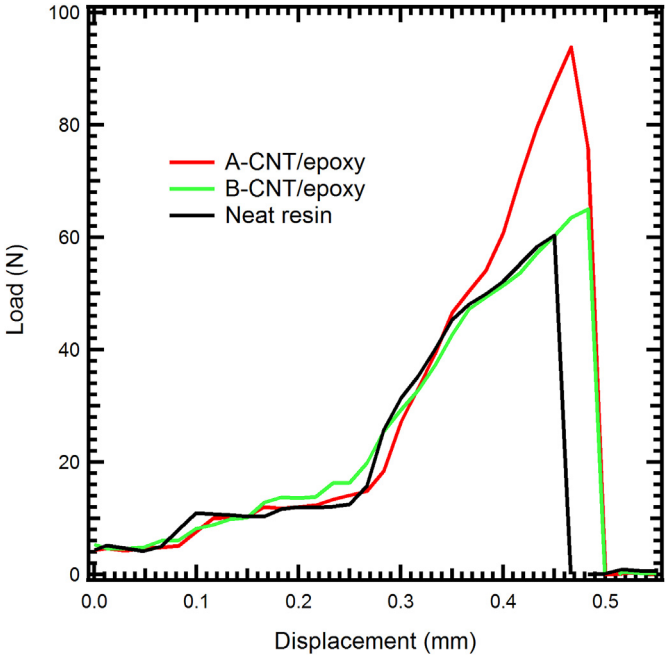

Fig. 4. Load displacement variation of neat resin and CNT/epoxy nanocomposite.

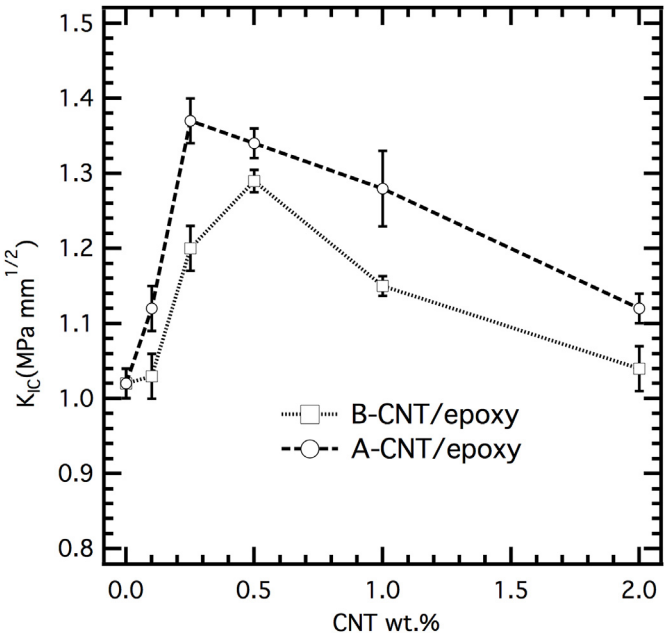

Fig. 5. Fracture toughness of neat resin and CNT/epoxy nanocomposite.

deviation. From the graph, it is plausible that the addition of CNT leads to an improvement in the value of the fracture toughness. After attaining a maximum value, the fracture toughness starts to decrease upon further addition of CNT. This could be due to the development of agglomerates of CNT particles at higher loading. For ball-milled CNT reinforced epoxy the fracture toughness increases by 29% at 0.5 wt% CNT reinforcement. APTMS-CNT modified epoxy exhibits an increase of 38% at 0.25 wt% epoxy.

This improvement in the value of fracture toughness implies that the presence of CNT increases the resistance against crack propagation which results in a more tortuous path. The higher value of fracture toughness for A-CNT/epoxy is due to two phenomena, (i) A-CNT dispersed better in the epoxy resin which results in increasing the resistance against crack propagation, and (ii) the APTMS work like a bridge between CNT and epoxy resin because hydrophobic part interact with CNT and hydrophilic part interact with epoxy resin which results in better CNT–matrix adhesion. Modification with the silane also increases the wettability of the CNT which results in better interaction with the epoxy resin compared to inert CNT. After attaining the maximum value of fracture toughness both B-CNT and A-CNT form agglomerates which lead to material deterioration of nanocomposite characterized by the formation of the microscopic size voids. These microscopic size voids become the critical site of failure and results in the decrease of fracture toughness value.

SEM analysis was conducted on the fracture surfaces of the nanocomposites as shown in Fig. 6 to further examine the failure mechanism. The crack propagation is from right to left for some images and from left to right in other images. The SEM images for neat resin shows regular surface indicating negligible resistance against crack propagation in the case of neat resin. The fracture surface of CNT reinforced epoxy shows more rough surface suggesting the presence of an external toughening mechanism due to the CNT. In all the images the presence of rivermark indicate the phenomena of crack arrest and release, indicating that the presence of stiffer CNT directs the crack into a more tortuous path. For A-CNT the number of rivermarks per scanned area and roughness is high suggesting that the CNT is uniformly distributed in the epoxy resin which leads to the high fracture toughness compared to B-CNT/epoxy. With higher CNT content in the A-CNT/epoxy, disconnected rivermarks can be observed which indicates that still at higher CNT loading the CNT is distributed very well. However,

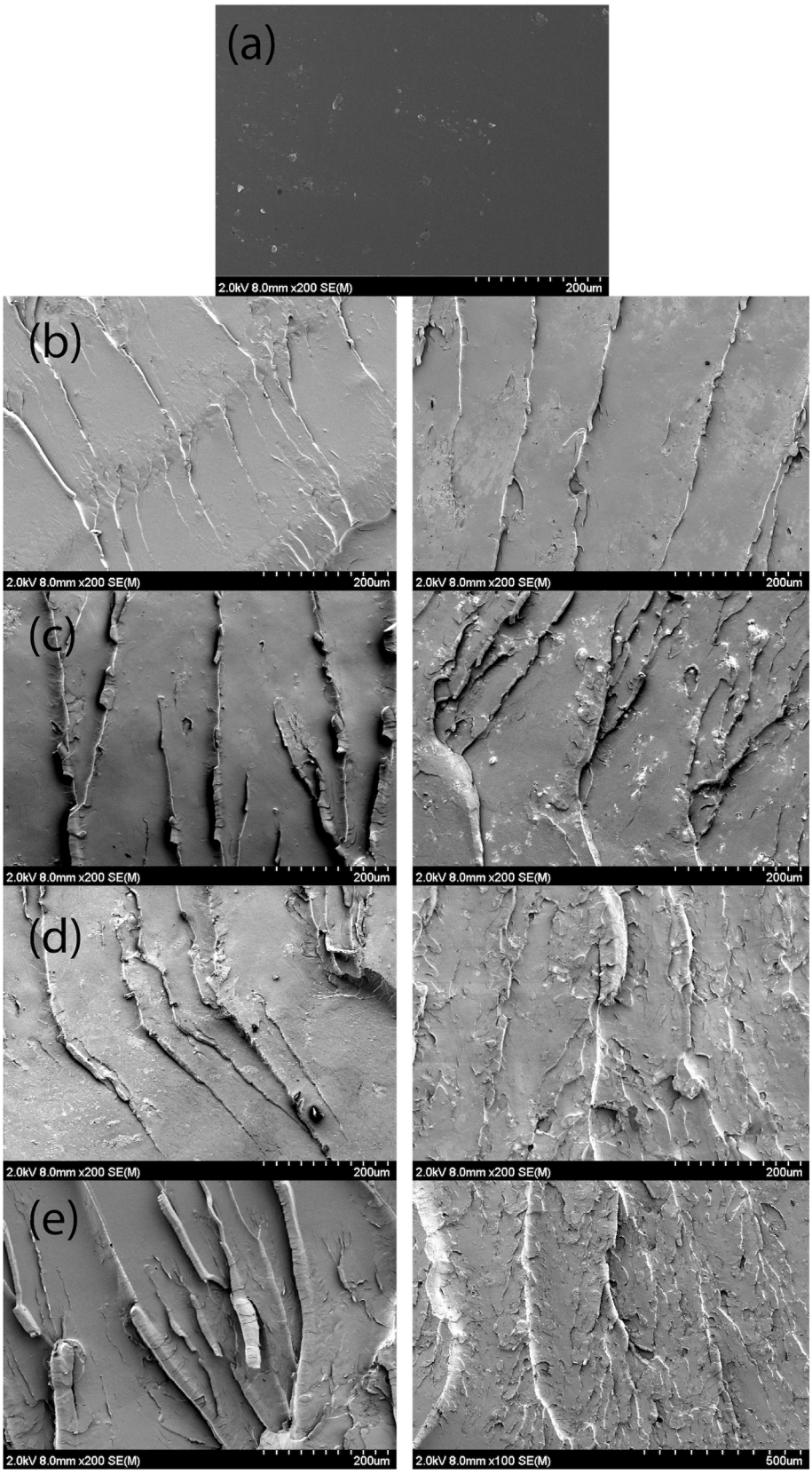

Fig. 6. Fractured morphology of (a) neat resin, CNT content in left (B-CNT/epoxy) and right (A-CNT/epoxy) (b) 0.1 wt%, (c) 0.5 wt%, (d) 1 wt% and (e) 2 wt%.

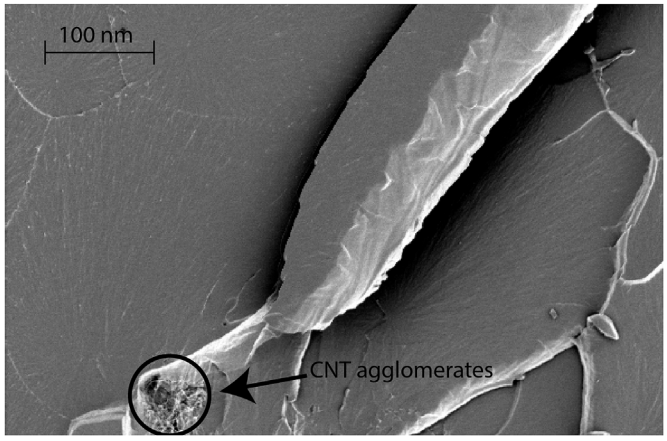

Fig. 7. Presence of agglomerates at 1 wt% B-CNT/epoxy shown at higher magnigication.

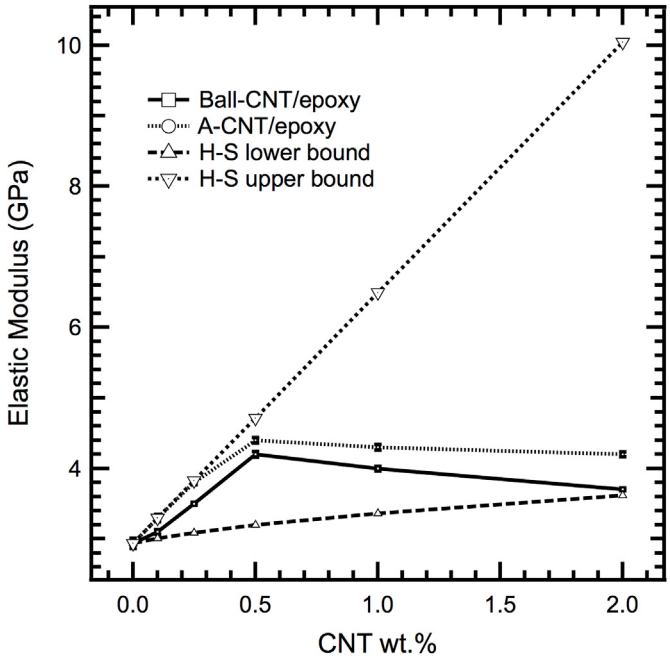

Fig. 8. Tensile modulus of A-CNT/epoxy and B-CNT/epoxy obtained from experiment, the modulus obtained comes between H–S bound.

for B-CNT epoxy the edge of rivermarks looked broken and folded suggesting the formation of agglomerates which results in the decrease in fracture toughness values. At higher magnification level as shown in Fig. 7, for 1 wt% B-CNT/epoxy the presence of agglomerates were observed as clumps-of-CNT that corresponds to the deleterious effect of agglomerates at the higher loading.

Fig. 8 shows the trend of elastic modulus similar to fracture toughness value with the inclusion of CNT. The elastic modulus first increases with CNT reinforcement then modulus decreases after attaining the maximum value. For B-CNT/epoxy, the modulus value increases and achieve maximum at 0.5 wt% with an increase of 36% compared to neat resin whereas for A-CNT/epoxy modulus values shows maximum values at 0.5 wt % by an increase of 42% compared to neat resin. This increase in the modulus value of the nanocomposite is due to the increase in the content of stiffer CNT nanoparticles. However, at higher CNT loading the nanoparticles produce agglomerates which leads to deterioration of the material. The higher value of modulus for A-CNT/epoxy compared to B-CNT/epoxy is due to the better wettability of CNT by silane which leads to the better CNT-matrix adhesion as well as, the better dispersion of CNT in the epoxy resin. The elastic modulus value for both case also comes between H–S lower and higher bounds (narrowest possible bounds). At lower CNT loading the trends follow the upper H–S bound whereas at higher loading it follows lower H–S bound.

Formation of CNT agglomerates was further investigated using transmission electron microscopy (TEM) on 1 wt% CNT loading. In Fig. 9, dark region denotes the presence of CNT and light region denotes the epoxy resin. As shown in Fig. 9, for B-CNT/epoxy the CNT bundles up and form CNT agglomerates of size around 300–350 nm. However, A-CNT/epoxy exhibit uniform dispersion of CNT with minimal formation of agglomerates. The results obtained from TEM can explain the effect of dispersion and functionalization quantitatively. However, to understand the formation of CNT agglomerates effectively and quantitatively at the nanoscale level we have performed the AFM indentation of the sample using contact mode.

As shown in Fig. 10. 0.5 wt% reinforced A-CNT/epoxy and B-CNT/epoxy were indented using AFM indenter and load-displacement curves were obtained from the indentation experiment. The slope from load-displacement curve used Oliver-Pharr method to calculate elastic modulus as shown in the equation below.

$$E_{OP} = \frac{1 - \nu_s^2}{\left(\frac{1}{E_r}\right) - \frac{(1-\nu_i^2)}{E_i}} \tag{4}$$

where ν_s is Poisson's ratio of the specimen, E_i and ν_i are elastic modulus and Poisson's ratio of the indenter. Where E_r is known as reduced modulus given by:

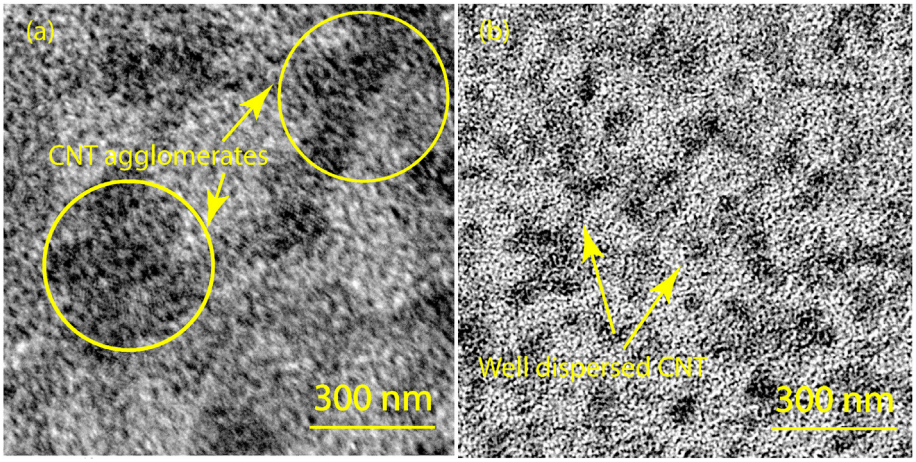

Fig. 9. Transmission electron microscopy of (a) A-CNT/epoxy and (b) B-CNT/epoxy exhibit the influence of CNT dispersion in the epoxy resin.

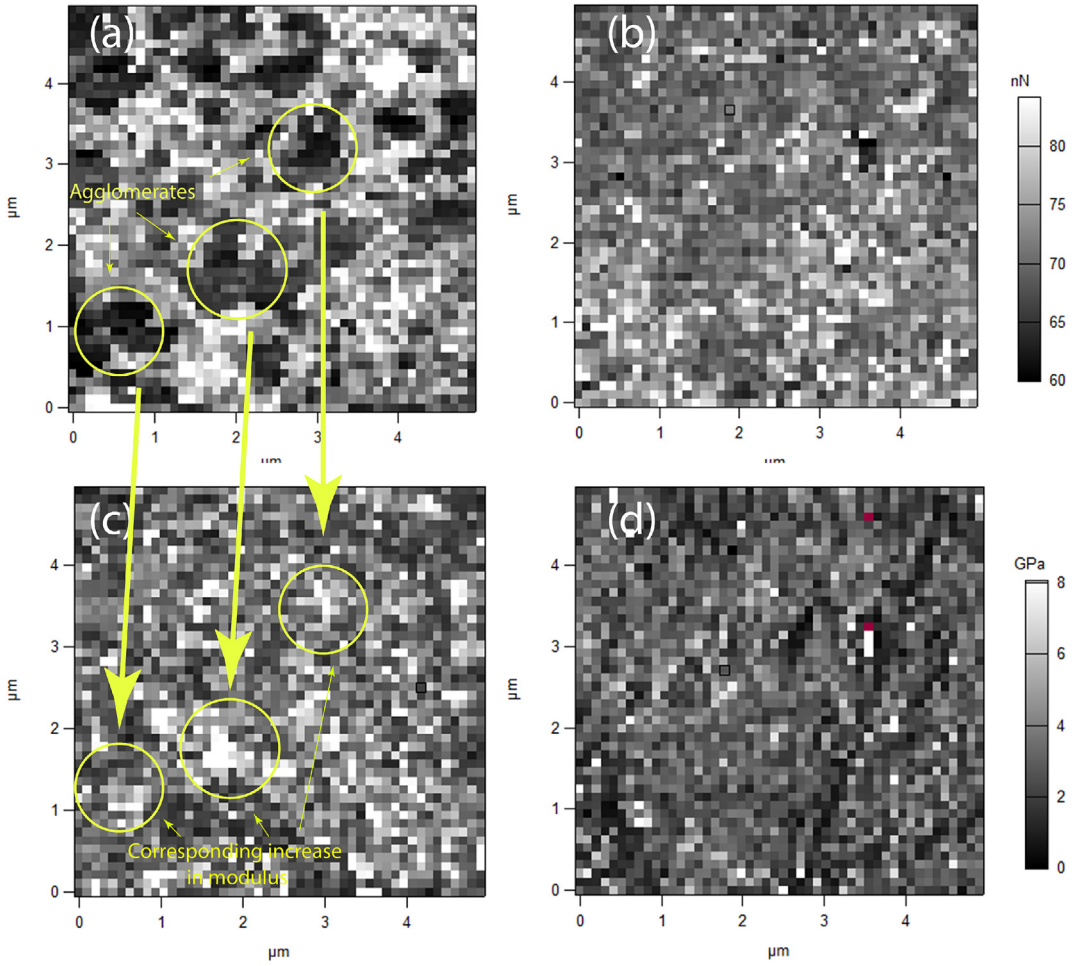

Fig. 10. (a)&(b) represents the adhesion map of B-CNT/epoxy and A-CNT/epoxy, adhesion map shows the evidence of agglomerates and (c)&(d) represents the elastic modulus maps corresponds to adhesion map.

Table 1
Average Modulus of 1 wt % CNT/Epoxy.

Material	Elastic Modulus
Neat resin	3.2± 0.8
0.1 wt% A-CNT/epoxy	3.8± 0.3
0.1 wt% B-CNT/epoxy	4.1± 0.4

$$E_r = \frac{\sqrt{\pi} S}{2\beta\sqrt{A_c}} \tag{5}$$

where β is known as correction factor usually the value of β is 1, A_c is known as the area of contact and S is the contact stiffness determined from the slope of the load-displacement curve, S is given by $S = \frac{dP}{dH}$.

Additionally, based on the interaction between indenter tip and sample, the adhesion map was also collected. From the adhesion map, we observed the formation of CNT agglomerates for B-CNT/epoxy whereas for A-CNT/epoxy there was no well-defined formation of agglomerates were evident at the scanning range. Elastic modulus map obtained from indentations shows pattern corresponds to the adhesion map. Very high elastic modulus was obtained at the location of agglomerates for B-CNT/epoxy as shown in Fig. 10 while in the case of A-CNT/epoxy due to the uniform dispersion of CNT leads to better adhesion between CNT and matrix, the uniform elastic modulus value was obtained. The average modulus from 2304 indentation points of B-CNT/epoxy and A-CNT/epoxy is shown in Table 1. Indentation on the neat resin was done for reference values. The average modulus from AFM indentation shows similar values obtained from the tensile experiment which indicates that the properties at local-scale can be translated well into bulk properties.

Table 2
Glass transition temperature of neat resin and CNT reinforced nanocomposites.

CNT loading	T_g	
	A-CNT/epoxy	B-CNT/epoxy
0	81.1 ± 1.1	81.1 ± 1.1
0.1	83.8 ± 1.0	84.1 ± 1.2
0.25	88.1 ± 1.5	92.2 ± 1.6
0.5	90.5 ± 1.1	99.2 ± 1.6
1	89.2 ± 2.1	93.2 ± 2.0
2	88.9 ± 1.8	92.8 ± 1.4

The effect of dispersion of CNT was further quantified using differential scanning calorimetry (DSC) as shown in Table 2. The presence of CNT shows the increase in the glass transition temperature which is due to the obstruction in the movement of the polymer chain by CNT. Increase in CNT-matrix interface, as well as better CNT dispersion due to silane modification, restrict the movement of polymer chain which eventually leads to a higher T_g values by 17.3% at 0.5 wt% compared to B-CNT reinforced epoxy where T_g increase by 11% at 0.5 wt%. Similar to the mechanical properties trend with the incorporation of CNT, the value of T_g also attains maximum then decreases due to the formation of CNT agglomerates.

4. Conclusion

In this study, the ball milled and silane modified of CNT reinforced epoxy resin was investigated. The treated A-CNT/epoxy and B-CNT/epoxy were characterized in terms of fracture toughness, tensile modulus, adhesion map, elastic modulus map and glass transition temperature. The significant finding from this investigation are discussed below:

1. Modification of silane on the CNT was confirmed from FTIR spectra.
2. A- CNT/epoxy exhibit greater fracture toughness by an improvement of 38% compared to neat resin whereas B-CNT/epoxy shows an improvement of 29%. Fractured surface morphology corroborates with the fracture toughness results.
3. The improvement in elastic modulus obtained from the tensile experiment was found higher for A-CNT/epoxy compared to B-CNT/epoxy and neat epoxy.
4. Effect of CNT dispersion or functionalization were reported qualitatively from transmission electron microscopy.
5. Adhesion map obtained from AFM indentation shows the evidence of agglomerates for B-CNT/epoxy compared to A-CNT/epoxy. Elastic modulus obtained from AFM confers similar values with the elastic modulus obtained from the tensile experiment.
6. Presence of CNT exhibit increase in glass transition temperature which corresponds to the better interfacial adhesion between epoxy and CNT.

Acknowledgements

This material is based upon work supported by the National Science Foundation under Grant No. 1649481.

References

[1] Pramanik Chandrani, Nepal Dhriti, Nathanson Michael, Gissinger Jacob R, Garley Amanda, Berry Rajiv J, Davijani Amir, Kumar Satish, Heinz Hendrik. Molecular engineering of interphases in polymer/carbon nanotube composites to reach the limits of mechanical performance. Compos Sci Technol 2018:0–1. April.
[2] Montazeri Arash, Khavandi Alireza, Javadpour Jafar, Tcharkhtchi Abbas. Viscoelastic properties of multi-walled carbon nanotube/epoxy composites using two different curing cycles. Mater Des 2010;31(7):3383–8.
[3] Kim Ki Seok, Rhee Kyong Yop, Lee Kyu Hwan, Byun Joon Hyung, Park Soo Jin. Rheological behaviors and mechanical properties of graphite nanoplate/carbon nanotube-filled epoxy nanocomposites. J Ind Eng Chem 2010;16(4):572–6.
[4] Bakhtiary Davijani Amir A, Chang Huibin, Clive Liu H, Luo Jeffrey, Kumar Satish. Stress transfer in nanocomposites enabled by poly(methyl methacrylate) wrapping of carbon nanotubes. Polymer 2017;130:191–8.
[5] Ayatollahi MR, Shadlou S, Shokrieh MM. Fracture toughness of epoxy/multi-walled carbon nanotube nano-composites under bending and shear loading conditions. Mater Des 2011;32(4):2115–24.
[6] Davijani Amir A Bakhtiary, Kumar Satish. Ordered wrapping of poly(methyl methacrylate) on single wall carbon nanotubes. Polymer 2015;70:278–81.
[7] Yu Bin, Jiang Zhenyu, Tang Xiu Zhi, Yue Chee Yoon, Yang Jinglei. Enhanced interphase between epoxy matrix and carbon fiber with carbon nanotube-modified silane coating. Compos Sci Technol 2014;99:131–40.
[8] Lee Ji Hoon, Rhee Kyong Yop, Lee Joong Hee. Effects of moisture absorption and surface modification using 3-aminopropyltriethoxysilane on the tensile and fracture characteristics of MWCNT/epoxy nanocomposites. Appl Surf Sci 2010;256(24):7658–67.
[9] Geng Yan, Liu Ming Yang, Li Jing, Xiao Mei Shi, Jang Kyo Kim. Effects of surfactant treatment on mechanical and electrical properties of CNT/epoxy nanocomposites. Compos Appl Sci Manuf 2008;39(12):1876–83.
[10] Yang Huafeng, Li Fenghua, Shan Changsheng, Han Dongxue, Zhang Qixian, Niu Li, Ivaska Ari. Covalent functionalization of chemically converted graphene sheets via silane and its reinforcement. J Mater Chem 2009;19(26):4632.
[11] Ma Peng Cheng, Kim Jang Kyo, Tang Ben Zhong. Effects of silane functionalization on the properties of carbon nanotube/epoxy nanocomposites. Compos Sci Technol 2007;67(14):2965–72.
[12] Albdiry MT, Yousif BF. Role of silanized halloysite nanotubes on structural, mechanical properties and fracture toughness of thermoset nanocomposites. Mater Des 2014;57:279–88.
[13] Kim MT, Rhee KY, Park SJ, Hui D. Effects of silane-modified carbon nanotubes on flexural and fracture behaviors of carbon nanotube-modified epoxy/basalt composites. Compos B Eng 2012;43(5):2298–302.
[14] Thomas Boris JC, Shaffer Milo SP, Aldo R, Boccaccini. Sol-gel route to carbon nanotube borosilicate glass composites. Compos Appl Sci Manuf 2009;40(6–7):837–45.
[15] Babu Libin K, Mishra Kunal, Hamim Salah U, Singh Raman P. Effect of excess silane on the viscoelastic behavior of epoxy under hygrothermal conditions. Int J Adhesion Adhes 2018;84(March):80–5.
[16] Vennerberg Danny, Hall Ryan, Kessler Michael R. Supercritical carbon dioxide-assisted silanization of multi-walled carbon nanotubes and their effect on the thermomechanical properties of epoxy nanocomposites. Polymer 2014;55(16):4156–63.
[17] Lee Ji Hoon, Kyong Yop Rhee, Park Soo Jin. Silane modification of carbon nanotubes and its effects on the material properties of carbon/CNT/epoxy three-phase composites. Compos Appl Sci Manuf 2011;42(5):478–83.
[18] ASTM D5045-14. Standard test methods for plane-strain fracture toughness and strain energy release rate of plastic materials 1. ASTM International 2013;99(1–9).
[19] ASTM D638. Standard test method for tensile properties of plastics. ASTM International 2003;08:46–58.
[20] Shrtirkman S, Hashin Z. A variational approach to the theory of the elastic behaviour of multiphase materials. J Mech Phys Solid 1963;11:127–40.